Dalton Transactions

ROYAL SOCIETY OF CHEMISTRY

PAPER

View Article Online
View Journal | View Issue

Cite this: *Dalton Trans.*, 2025, **54**, 3796

Hydrothermal growth and characterization of large Rb_2SnBr_6 double perovskite crystals: a promising semiconductor material for photocatalysis and optoelectronics†

Rahidul Hasan, Hafiz Zohaib Aslam, Rutva Joshi, Roger A. Lalancette and Georgiy Akopov *

Received 24th September 2024,
Accepted 21st January 2025

DOI: 10.1039/d4dt02712d

rsc.li/dalton

In this study, we present the growth of large (millimeter- and centimeter-scale) crystals of Rb_2SnBr_6 double perovskite *via* a hydrothermal process. The crystals and powders were successfully synthesized, yielding light-yellow products, and subjected to comprehensive characterization using powder and single crystal X-ray diffraction (XRD), energy-dispersive spectroscopy (EDS) point analysis, and UV-Vis diffuse reflectance spectroscopy. Previously, methods such as solution growth, evaporation, and gel techniques have been employed to synthesize Rb_2SnBr_6. However, none of these approaches have successfully yielded large crystals on the millimeter- or centimeter-scale. Our experimental results reveal that Rb_2SnBr_6 is a semiconductor with a bandgap of 2.97 eV. This wide bandgap not only suggests high stability and low defect levels but also positions Rb_2SnBr_6 as a highly promising candidate for advanced applications in photocatalysis, photovoltaics, and optoelectronics. The ability to grow large-sized crystals with such favorable electronic properties highlights the material's potential for integration into scalable technologies, paving the way for further research and development in energy conversion and optoelectronic devices.

Introduction

Double halide perovskites, represented by the general formula A_2BX_6 (A = alkali-earth metals, B = transition metals, and X = halide), have emerged as a fascinating class of materials due to their diverse structural properties and extensive potential applications.[1,2] These materials have garnered significant attention for their roles in photocatalysis,[3] optoelectronics,[4] photovoltaics,[5] thermoelectric,[6] and nonlinear optical devices[7] owing to their unique electronic, optical, and magnetic characteristics. These materials exhibit a unique crystal structure that contributes to their high absorption coefficients, long carrier diffusion lengths, and tunable bandgaps, making them ideal candidates for various applications, notably in photovoltaic cells and light-emitting devices.[8] Even though stability is the main issue with halide perovskite, many are very stable at ambient temperature. Stability is a primary concern, as these materials can degrade under environmental stressors like moisture, heat, and ultraviolet light.[9,10] Additionally, the presence of lead in most high-performing perovskites poses environmental and health risks, necessitating the development of lead-free alternatives.[11,12]

Current research focuses on improving the stability of halide perovskites through compositional engineering, surface passivation, and encapsulation techniques.[13] Moreover, significant efforts are being made to discover and develop non-toxic, lead-free perovskites that do not compromise performance.[14] Lead-free halide perovskites are emerging as a promising alternative to traditional lead-based perovskites, addressing environmental and health concerns of lead toxicity. These materials seek to retain the desirable properties of lead halide perovskites, such as high absorption coefficients, long carrier lifetimes, and tunable bandgaps, while eliminating the harmful effects of lead. Lead-free halide perovskites typically replace lead with other metals such as tin, germanium, bismuth, and antimony.[14–18] Among these, tin-based perovskites are the most studied due to their structural similarity to lead perovskites and their promising optoelectronic properties.[19,20] Despite their potential, Sn-based perovskite optoelectronic devices still underperform compared to their lead counterparts.[21] Sn perovskites differ from their Pb

Department of Chemistry, Rutgers University – Newark, Newark, NJ 07102, USA. E-mail: georgiy.akopov@rutgers.edu

†Electronic supplementary information (ESI) available: Additional experimental details of the hydrothermal synthesis, powder XRD, EDS, and TGA data. CCDC 2381629 and 2381630. For ESI and crystallographic data in CIF or other electronic format see DOI: https://doi.org/10.1039/d4dt02712d

counterparts in that they are prone to oxidation, attributed to their different $5s^2p^2$ configuration and, thus, the lack of lanthanide contraction.[13] Therefore, Sn(II) is converted to Sn (IV) more readily when it is exposed to oxidation sources such as oxygen or solvents like dimethyl sulfoxide (DMSO).[22] As a result, synthesizing stable single tin halide perovskites, like $ASnX_3$, remains highly challenging. This has led to vacancy-ordered double perovskites, such as A_2SnX_6, emerging as promising alternatives.[23,24]

Among the tin-based A_2SnX_6 (A = K, Rb, Cs; and X = Cl, Br, I) families, there are a few experimental reports on Rb_2SnBr_6. The first experimental report, by Costeanu *et al.*, came out in 1927[25] after that, Ketelaar *et al.*[26] described the crystal structure of Rb_2SnBr_6 using XRD analysis. The third report was published in 1980 by Suib *et al.*[27] synthesize Rb_2SnBr_6 using a gel process. Numerous theoretical studies of Rb_2SnB_6 have been published since.[6,28–32] In 2022, Ganesan *et al.*[33] reported a synthesis of nanocrystals of Rb_2SnBr_6 double perovskite nanocrystals by the evaporation process. Furthermore, their targeted materials were synthesized $RbSnBr_3$ nanocrystals, which spontaneously oxidized to stable Rb_2SnBr_6 nanocrystals. Finally, in 2023, Glockzin *et al.*, directly synthesized Rb_2SnBr_6 powder by an evaporation process.[34] The synthesis of Rb_2SnBr_6 double perovskite might have been underreported for several reasons, one of which is the poor stability of Sn-based perovskites. Tin can readily oxidize from Sn^{2+} to Sn^{4+}, leading to the degradation of the resulting materials. This instability can make it challenging to synthesize and study these materials in a reproducible manner.[22] The synthesis of high-quality Rb_2SnBr_6 can be more challenging compared to other perovskites. Factors like the precise control of stoichiometry, temperature, and atmosphere during synthesis can be more demanding, leading to fewer successful reports. Researchers may prioritize other lead-free perovskite materials that offer better stability and more accessible synthesis, such as bismuth or antimony-based perovskites. These materials might be more attractive due to their potentially better performance and stability.[35,36]

We successfully synthesized the Rb_2SnBr_6 millimeter and centimeter-sized large crystals using a one-step hydrothermal process. We were initially motivated to grow $Rb_4Sn_3Br_2I_8$ from the work of Gong *et al.*,[37] who synthesized $Rb_4Sn_3Cl_2Br_8$ for the optoelectronic application. However, our analysis revealed that instead of forming the $Rb_4Sn_3(Br_2I_8)$ phase, it formed $Rb_2Sn(Br_{5.5}I_{0.5})$, which indicates that Rb_2SnBr_6-type perovskite is the more favorable product in this quaternary system. We later synthesized the Rb_2SnBr_6 phase using a stoichiometric amount of precursors. Going forward, we will use (Rb : Sn : X) ratio notation to indicate the nominal stoichiometry used where relevant: Rb_2SnBr_6 (2 : 1 : 6) or Rb_2SnBr_6 (4 : 3 : 10).

Experimental procedure

Chemicals

Doped and pristine Rb_2SnBr_6, Rb_2SnCl_6, and Rb_2SnI_6 were synthesized using a one-step hydrothermal synthesis technique. The chemicals used for the synthesis are: RbBr (99%, Strem), RbCl (99.8%, Sigma-Aldrich), RbI (99.9%, Sigma-Aldrich), $SnBr_4$ (99%, Sigma-Aldrich), $SnBr_2$ (99.2%, ThermoFisher), $SnCl_4$ (98%, Sigma-Aldrich), SnI_4 (99%, ThermoFisher), HBr (48%, Sigma-Aldrich), HCl (37%, VWR) and HI (57%, Sigma-Aldrich). All chemicals utilized in this process are employed without further purification.

Hydrothermal synthesis

Two compositions were selected for the study: Rb_2SnBr_6 (2 : 1 : 6) and $Rb_4Sn_3Br_{10}$ (4 : 3 : 10). Stoichiometric amounts of RbBr and $SnBr_4$ were measured into a 25 mL Teflon liner within a glove box due to $SnBr_4$'s hygroscopic nature. Subsequently, 2.0 mL of an HBr solution ($HBr : H_2O$ = 1 : 3) was added to the mixtures. The role of HBr is to maintain the acidic condition of the system. The Teflon liner was then sealed within a stainless-steel autoclave and placed in a furnace. The temperature was maintained at 220 °C for 24 hours, followed by a gradual reduction of 3 °C per hour to promote the growth of finer crystals. Light yellow crystals of millimeter size were extracted from the $Rb_4Sn_3Br_{10}$ (2 : 1 : 6) composition, while yellow crystals of centimeter size were obtained from Rb_2SnBr_6 (4 : 3 : 10). The reaction for the formation of Rb_2SnX_6 is given below:

$$2RbX + SnX_4 + HX_{solution} \rightarrow Rb_2SnX_6 + HX + H_2O \quad (X = Cl, Br, \text{and } I) \quad (1)$$

Powder XRD

PXRD characterization was performed using a Rigaku Miniflex 600 diffractometer employing Cu-Kα radiation (λ = 1.5434 Å). The sample holders were comprised of zero-background silicon plates. The finely ground sample powders were placed on round sample holders and pressed with a glass slide to secure the samples. Diffraction measurements were taken while rotating the sample holder at 15 rpm. The Rietveld refinement was done using the open-source Python package Py-GASA-II, developed by Brian Toby from Argonne National Laboratory.[38]

Single crystal XRD

SCXRD data were collected on a Rigaku XtaLAB Synergy-S Dual Source diffractometer equipped with a PhotonJet Mo-microfocus source (λ = 0.71073 Å) and a HyPix-6000HE detector. Data reduction was performed with CrysAlisPro 65; subsequent data processing was also performed in CrysAlisPro. Using the SCALE3 ABSPACK scaling algorithm 66, empirical absorption corrections were applied to the data. Empirical and numerical (Gaussian) absorption corrections, determined by face-indexing and integration, were applied to the data. The structure was solved by applying the intrinsic phasing in SHELXT and refined by full-matrix least-squares techniques against F^2 (SHELXL) in the Olex2 graphical user interface.[39]

Diffuse-reflectance

The bandgaps were calculated from UV-Vis absorption spectra using Tauc plots. UV-Vis measurements of the finely ground powder samples were performed with a Cary 5000 UV-Vis-NIR instrument, using KBr as a standard reference sample.

EDS

The energy-dispersive X-ray spectroscopy (EDS) point analysis was done by a Hitachi S-4800 high resolution scanning electron microscopy. The voltage, current and magnification were used 15 kV, 20 mA and 5000× for EDS measurement. Generally, we chose one spot for the EDS point; however, 3 spots were also chosen for the pristine Rb_2SnBr_6.

Thermogravimetric analysis

Thermogravimetric analysis (TGA) was performed using the Water™ Discovery TGA 5500 instrument. TGA was performed on the single crystals of Rb_2SnBr_6 (2 : 1 : 6) and Rb_2SnBr_6 (4 : 3 : 10) under a nitrogen atmosphere in a Platinum pan. The temperature range for the TGA measurement was set from 0 °C to 1000 °C.

Results and discussion

Rb_2SnBr_6 exhibits a face-centered cubic structure with the space group $Fm\bar{3}m$ (space group #225), which corresponds to the K_2PtCl_6 structure type. Typically, halide double perovskite compounds with the formula A_2BX_6 exhibit a vacancy-ordered structure characterized by isolated [BX_6] octahedra that form a 12-fold coordination environment with discrete X anions. In this arrangement, A atoms are coordinated by 12 halide atoms, and B atoms are coordinated by 6 halide atoms, resulting in a face-centered cubic crystal structure (Fig. 1).

The synthesis of air- and moisture-stable Rb_2SnBr_6 presents significant challenges, as evidenced by the scarcity of published experimental data. To date, only four experimental studies on Rb_2SnBr_6 halide double perovskite have been reported.[25–27,33] Although several theoretical studies on Rb_2SnBr_6 predict various properties such as photocatalysis, thermoelectricity, optoelectrical behavior, and photoluminescence,[4–6] the limited experimental data have impeded the validation of these properties. Here we present the first to report the successful growth of large crystals of Rb_2SnBr_6 double perovskite, ranging from millimeter to centimeter scales.

The successful synthesis of large crystals of Rb_2SnBr_6 double perovskite was achieved *via* a hydrothermal process. Details for the synthesized crystals can be seen in Table 1. Traditionally, tin(II) bromide ($SnBr_2$) is employed in the synthesis of Rb_2SnBr_6; however, the oxidative nature of Sn leads to the oxidation of Sn(II) to Sn(IV) in ambient conditions.[22] To mitigate this issue, $SnBr_4$ was used instead of $SnBr_2$, yielding remarkable results. We successfully synthesized several batches of air- and moisture-stable large crystals of Rb_2SnBr_6, ranging from millimeters to centimeters in size (Fig. 2). The as-synthesized Rb_2SnBr_6 is light yellow; however, Cl and I-doping on the Br site change colors from yellow to dark yellow and dark orange, respectively (Fig. 2). A few inclusions can be observed with naked eye with a length of 0.5–4 mm (approximately 5 to 10% of the total crystal volume (Fig. S1†)); however, we could not determine with full certainly if they are

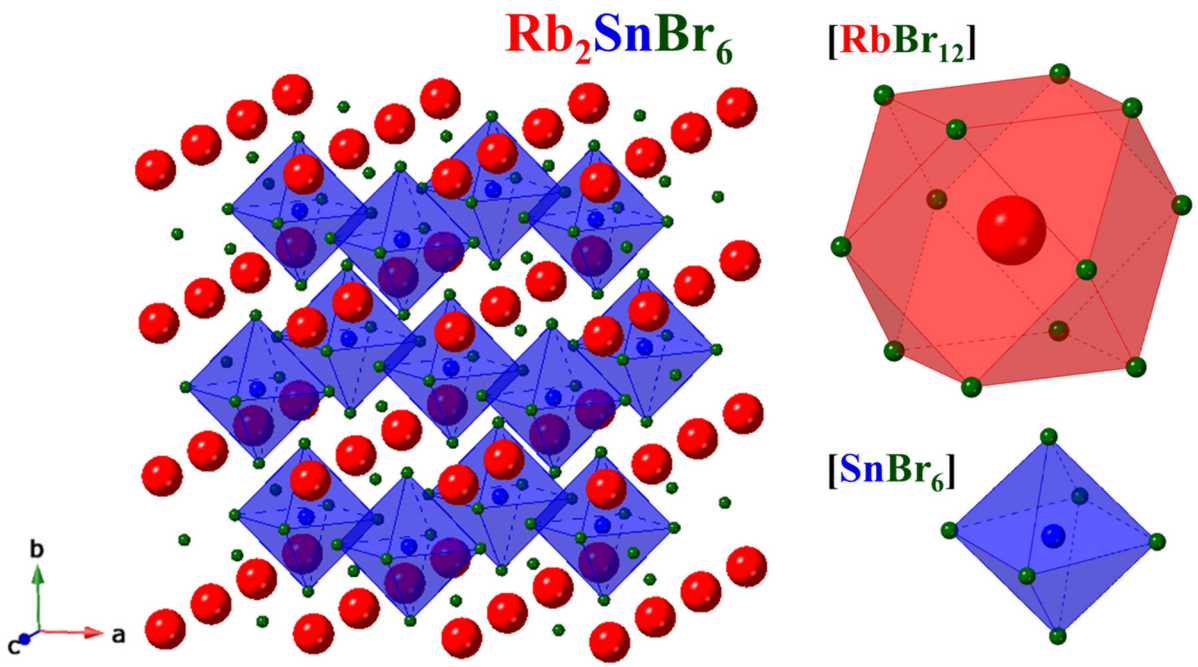

Fig. 1 Crystal structure of Rb_2SnB_6 ($Fm\bar{3}m$), showing the polyhedral filling with the 12-sided [$RbBr_{12}$] prism and [SnB_6] tetrahedra.

Table 1 Crystallographic data for the halide perovskite crystals

Phase	Rb_2SnCl_6 (2 : 1 : 6)	Rb_2SnBr_6 (2 : 1 : 6)
CSD-number	2381630	2381629
Space group	$Fm\bar{3}m$	
λ (Å)	Mo-Kα: 0.71073	
T (K)	105(2)	101(2)
a (Å)	10.0195(1)	10.5767(6)
V (Å^{-3})	1005.86(3)	1183.2(2)
Z	2	
ρ (g cm^{-3})	3.317	4.317
Absorption correction	Multi-scan	
μ (mm^{-1})	13.671	30.531
θ (°)	$3.49 < \theta < 53.74$	$3.34 < \theta < 46.11$
Data/param.	364/6	121/6
R_1	1.62	3.01
wR_2	3.73	6.86
Goodness-of-fit	1.137	1.247
Diff. peak/hole (e Å^{-3})	1.592/−1.491	1.558/−1.908

single or poly-crystalline domains (Fig. S1†). Using optical microscopy faceting could not be detected in the domains. There was no evidence of this domain formation in 10% Cl-doped $Rb_2SnBr_{5.4}Cl_{0.6}$ crystal, suggesting that 10% Cl-doping might promote defect-free crystal growth. In order to grow such large single crystals of better quality it would be important to precisely control the synthesis and cooling temperatures, changing the solvent concentration, and introducing a seed crystal growing technique.

The synthesis of Rb_2SnBr_6 crystals requires careful control of growth and nucleation to produce high-quality materials with desirable properties. Key factors include adjusting precursor concentrations, temperature, solvent conditions, and growth kinetics. High supersaturation encourages nucleation, leading to multiple tiny crystals, while lower supersaturation promotes the growth of larger crystals. Maintaining an optimal precursor ratio ($RbBr : SnBr_4$) is crucial, as excessive tin precursor concentration can induce nucleation. Temperature control is essential, with lower temperatures suppressing nucleation and higher but controlled temperatures promoting growth. Solvents like DMF or ethylene glycol ensure controlled supersaturation, while crystallographic factors influence the development of defined facets. Post-synthesis treatments such as annealing can further refine crystal quality. By balancing these factors, we can produce Rb_2SnBr_6 crystals with controlled sizes and minimal defects.

Initially, our research aimed at synthesizing $Rb_4Sn_3Br_2I_8$ perovskite materials; however, Rb_2SnBr_6 emerged as the more favorable phase for this synthesis technique. We synthesized a series of Rb_2SnX_6 (X = Cl, Br, and I) double perovskites and characterized them using single crystal X-ray diffraction (SXRD) and powder crystal X-ray diffraction (PXRD). The PXRD results matched the reference data set ICSD-158956, as shown in Fig. 3. In addition, we doped Rb_2SnBr_6 (2 : 1 : 6) with Cl and I and characterized by Rietveld refinement, PXRD (Fig. S2 and Table S2†), and EDS point analysis (Fig. S3 and S4†). Our effort to synthesize the double perovskite $Rb_4Sn_3Br_2I_8$ ultimately produced $Rb_2SnBr_{5.5}I_{0.5}$, which was confirmed by SCXRD as well as a peak shift to lower angles in the PXRD (Fig. S5†) data. The Rietveld refinement of the powder crystal XRD also confirms the successful formation of the Rb_2SnBr_6 (Fig. 3).

In addition to validating previous experimental techniques, we attempted to synthesize Rb_2SnBr_6 perovskite using an evaporation process previously reported by Ganesan *et al.*[33] at 120 °C. We utilized both $SnBr_2$ and $SnBr_4$ as the sources of tin. Our experimental results indicate that evaporation can only produce micron-sized powders (Fig. S6 and S7†). The powder XRD analysis revealed the formation of $RbSnBr_6$ phases mixed with the corresponding raw materials phase of $SnBr_2$ and

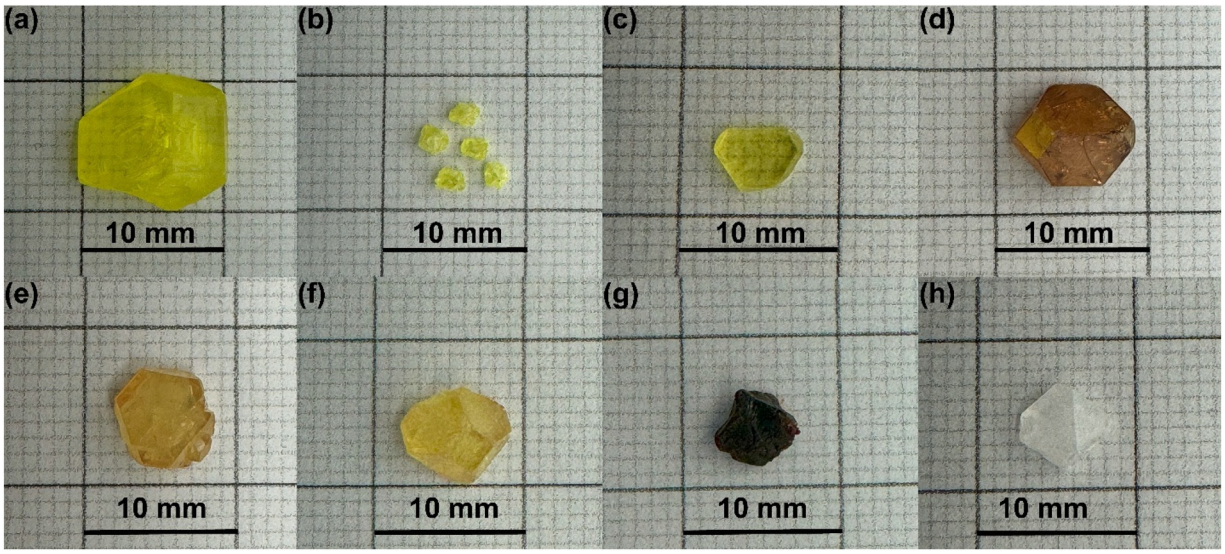

Fig. 2 Images of as-synthesized centi- and millimeter-sized single crystals of pristine and doped Rb_2SnBr_6: (a) Rb_2SnBr_6 (4 : 3 : 10), (b) Rb_2SnBr_6 (2 : 1 : 6), (c) $Rb_2SnBr_{5.4}Cl_{0.6}$ (2 : 1 : 6) (d) $Rb_2SnBr_{4.5}Cl_{1.5}$ (2 : 1 : 6), (e) $Rb_2SnBr_3Cl_3$ (2 : 1 : 6) (f) $Rb_2SnBr_{1.5}Cl_{4.5}$ (2 : 1 : 6) (g) $Rb_2SnBr_{5.5}I_{0.5}$ (4 : 3 : 10)(h) Rb_2SnCl_6 (2 : 1 : 6).

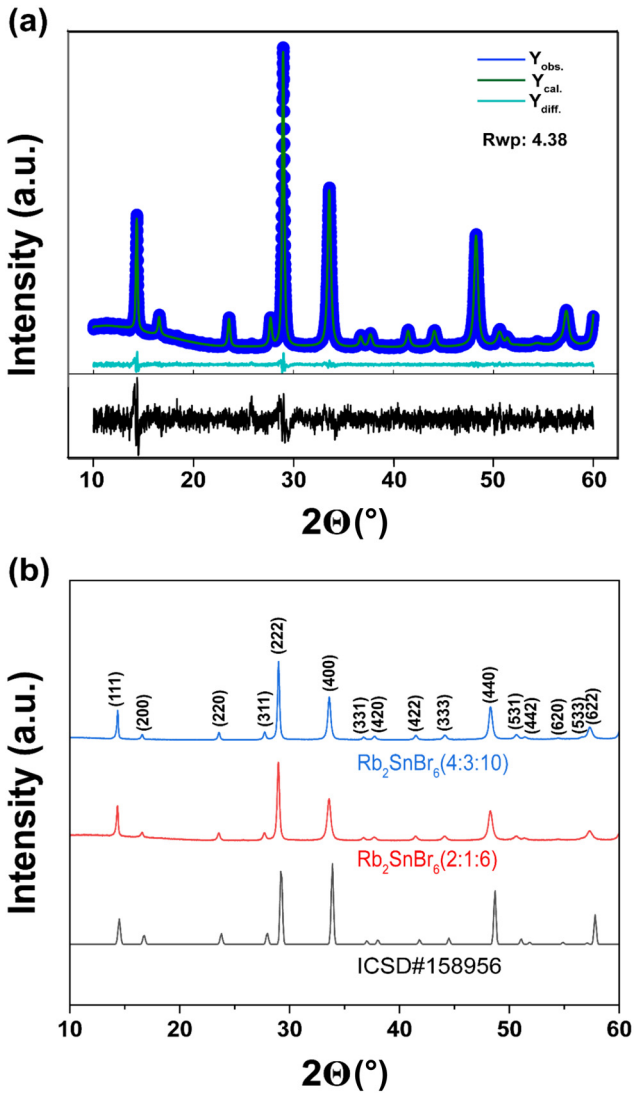

Fig. 3 Analyzed powder XRD data: (a) Rietveld refinement plot of the Rb_2SnBr_6 (4 : 3 : 10) double perovskite halide. Rietveld refinement data: $Fm\bar{3}m$, a = 10.678 Å, V = 1217.71 Å^3, R_{wp} = 4.38%, and (b) powder crystal XRD of Rb_2SnBr_6 (2 : 1 : 6) and Rb_2SnBr_6 (4 : 3 : 10), which are a close match to each other.

$SnBr_4$. Moreover, our hydrothermal study for the fabrication of large Rb_2SnBr_6 crystals produces a similar result at 150 °C. The formation of the halide double perovskite was confirmed by comparing the PXRD data with reference standards (ICSD#158956). The synthesized Rb_2SnBr_6 appeared light yellow when $SnBr_4$ was used, but it turned dark orange when $SnBr_2$ was the tin source. We tried to synthesize Rb_2SnBr_6 perovskite at 120 °C by the hydrothermal process; however, the reaction was relatively unsuccessful, with the majority of products being unreacted reactants (Fig. S8†). It can be concluded that 120 °C is not enough for the reaction to reach the optimum pressure to facilitate the reaction and grow the crystals by hydrothermal process. We compare and arrange several synthesis techniques previously applied to fabricate Rb_2SnBr_6 crystals in Table S1.†

Meanwhile, we were successfully able to synthesize colorless crystals of Rb_2SnCl_6 double perovskite, however, our efforts to grow stable Rb_2SnI_6 crystals were unsuccessful. Although we managed to produce yellow, needle-like crystals of Rb_2SnI_6, they degraded to black crystals within 24 hours when exposed to air. Despite numerous experimental reports of nano- and micron-sized Rb_2SnCl_6, our large sample demonstrated excellent stability in air and moisture. SCXRD and PXRD analyses confirmed the successful formation of the cubic phase of Rb_2SnCl_6 double perovskite (Table 1 and 2 and Fig. S9†).

Through numerous experimental iterations, we successfully synthesized large crystals in each successful attempt. However, some of these crystals exhibited twining properties. To confirm the formation of the target phase, we performed elemental analysis using energy-dispersive X-ray spectroscopy, which showed a close match with the nominal composition $Rb_{2.2(2)}Sn_{1.04(4)}Br_{5.51(44)}$ (Fig. S11†).

We calculated the optical bandgap of the synthesized compounds, as shown in Fig. S12.† The UV-Vis absorption data were used to calculate the bandgap using the Tauc equation:

$$(\alpha h\nu)^{1/n} = A(h\nu - E_g) \quad (2)$$

where α is the absorption coefficient, h is Planck's constant, ν is the frequency, A is a proportional constant, and E_g is the optical bandgap energy.

The direct and indirect bandgaps of the pristine and doped samples are displayed in Fig. S12.† The calculated data indicate that both pristine and doped Rb_2SnBr_6 halide double perovskites possess bandgaps of close to 3 eV, making them promising candidates for applications in photocatalysis, optoelectronics, thermoelectric, and photoluminescence (PL). We present both direct and indirect bandgaps in Fig. S12† but we do not claim these perovskites to be direct-band gap semiconductors without further investigation. The pristine Rb_2SnBr_6, which is light yellow in color, has a bandgap of 2.97 eV, consistent with the literature. The direct bandgap of I-doped $Rb_2SnBr_{5.5}I_{0.5}$ (2 : 1 : 6) is reduced to 2.29 eV, corresponding to its color spectrum. The bandgap of Cl-doped $Rb_2SnBr_3Cl_3$ (2 : 1 : 6) increased to 3.14 eV due to the presence of Cl even though the intrinsic Rb_2SnCl_6 has a direct bandgap of 4.42 eV. Replacing Br with Cl decreases the ionic radius. Consequently, lattice contraction takes place. Replacing halogen introduces the nephelauxetic effect, which reduces the effective nuclear charge of the host system. It could be one of the major points in reducing the bandgap of 50% Cl-doped $Rb_2SnBr_3Cl_3$ (2 : 1 : 6).

In addition, we performed the thermogravimetric analysis (TGA) of both samples Rb_2SnBr_6 (2 : 1 : 6) and Rb_2SnBr_6 (4 : 3 : 10) (Fig. S13†) from 0 °C to 1000 °C. It reveals that both the centi- and millimeter-sized Rb_2SnBr_6 crystals are stable to around 300 °C, and then begin to decompose. Rb_2SnBr_6 (2 : 1 : 6) started to decompose at 303.45 °C while the decomposition of Rb_2SnBr_6 (4 : 3 : 10) started at 376 °C. A phase transition seems to be occurred for Rb_2SnBr_6 (2 : 1 : 6) at 304 °C. At

Table 2 Several synthesis techniques for the growing of Rb_2SnBr_6 halide perovskite single crystal

Single crystal growing process	Gel growth	Evaporation	Solution	Hydrothermal
Ref.	27	33	26	Current work
Precursor materials	RbBr (aq.), $SnBr_3/SnBr_4$, CH_3COOH	RbBr, $SnBr_2$	RbBr, $SnBr_2$	RbBr, $SnBr_4$, HBr
Solvent	H_2O	H_2O/DMF	H_2O	H_2O
Temperature (°C)	25–65	120	150	220
Crystal size	Millimeter	Nano	Unknown	Milli to centimeter
Phase	Cubic ($Fm\bar{3}m$)	Cubic ($Fm\bar{3}m$)	Cubic ($Fm\bar{3}m$)	Cubic ($Fm\bar{3}m$)
Crystal color	Yellow white	White	Yellow	Light yellow
Yield percentage	Unknown	Unknown	Unknown	70–80%

close to 500 °C, both of them lose more than 50% of their total weight. After increasing the temperature, the decomposition continues, and at the end of 1000 °C, 13.46% of Rb_2SnBr_6 (2 : 1 : 6) and 4.5% of Rb_2SnBr_6 (4 : 3 : 10) remain.

Conclusion

Our experimental results and subsequent data analysis demonstrate the successful fabrication of large milli- and centimeter-sized Rb_2SnBr_6 halide double perovskite *via* the hydrothermal process. Powder X-ray diffraction (PXRD) and single-crystal X-ray diffraction (SXRD) analyses confirmed the formation of the cubic structure with the space group $Fm\bar{3}m$ (number 225). PXRD and energy-dispersive X-ray spectroscopy (EDS) elemental analysis verified the successful formation of Rb_2SnBr_6. All Cl- and I-doped Rb_2SnBr_6 halide double perovskites demonstrated stability in air and moisture. The optical bandgap, calculated from absorption data, indicates wideband semiconductor properties, suggesting potential applications in photocatalysis, electrocatalysis, optoelectronics, and photoluminescence. Due to time constraints, we were unable to test the physical properties and applications of these crystals. Our future work will focus on investigating the photocatalytic and electrocatalytic activities of Rb_2SnBr_6 halide double perovskite.

Author contributions

The manuscript was written through the contributions of all authors.

Data availability

Additional experimental details of the hydrothermal synthesis, PXRD, EDS, UV-Vis diffuse-reflectance, and TGA data. Further details of the crystal structure investigations may be obtained from the joint CCDC/FIZ Karlsruhe by quoting the CSD deposition numbers: 2381629 and 2381630.†

Conflicts of interest

There are no conflicts to declare.

Acknowledgements

This research was supported by a Rutgers University, Newark startup grant (R. H., H. Z. A., R. J., G. A.). The X-ray diffractometer was purchased with support from the National Science Foundation Grant No. [2018753] (R. A. L.).

References

1 P.-K. Kung, M.-H. Li, P.-Y. Lin, J.-Y. Jhang, M. Pantaler, D. C. Lupascu, G. Grancini and P. Chen, Lead–Free Double Perovskites for Perovskite Solar Cells, *Sol. RRL*, 2020, **4**, 1900306.
2 W. Rahim, A. Cheng, C. Lyu, T. Shi, Z. Wang, D. O. Scanlon and R. G. Palgrave, Geometric Analysis and Formability of the Cubic A_2BX_6 Vacancy-Ordered Double Perovskite Structure, *Chem. Mater.*, 2020, **32**, 9573–9583.
3 S. S. Padelkar, Vikram, J. J. Jasieniak, A. N. Simonov and A. Alam, Mixed-halide vacancy-ordered double perovskite for photovoltaic and photocatalysis applications, *Phys. Rev. Appl.*, 2024, **21**, 044031.
4 M. Faizan, X. Wang, S. A. M. Abdelmohsen, K. C. Bhamu, S. Sappati, A. Laref, N. Muhammad, M. Mushtaq, A. M. M. Abdelbacki and R. Khenata, Understanding the Electronic Structure and Optical Properties of Vacancy-Ordered Double Perovskite A_2BX_6 for Optoelectronic Applications, *Energy Fuels*, 2022, **36**, 7065–7074.
5 M. A. Kinani, R. Chami, A. Lekdadri, A. ElRharib, Y. Mir, E. K. Hlil, A. Amine and M. Zazoui, Structural, electronic and optical properties of A_2SnBr_6 (A = K, Cs, and Rb) for photovoltaic applications: First-principles calculation, *Comput. Condens. Matter*, 2021, **26**, e00520.
6 A. El Rharib, A. Amine, A. Oukerroum, M. A. Kinani, Y. Mir and M. Zazoui, Improved thermoelectric, thermodynamic, and optical properties performance of double perovskites A_2SnBr_6 (A = Cs, K, Rb) from first-principles calculations, *Comput. Condens. Matter*, 2022, **33**, e00744.
7 H. Z. Aslam, J. T. Doane, M. T. Yeung and G. Akopov, Advances in Solid-State Nonlinear Optical Materials: From Fundamentals to Applications, *ACS Appl. Opt. Mater.*, 2023, **1**, 1898–1921.
8 M. Huma, M. Rashid, Q. Mahmood, E. Algrafy, N. A. Kattan, A. Laref and A. S. Bhatti, Physical properties

of lead-free double perovskites A_2SnI_6 (A = Cs, Rb) using *ab initio* calculations for solar cell applications, *Mater. Sci. Semicond. Process.*, 2021, **121**, 105313.

9 T. Leijtens, G. E. Eperon, N. K. Noel, S. N. Habisreutinger, A. Petrozza and H. J. Snaith, Stability of Metal Halide Perovskite Solar Cells, *Adv. Energy Mater.*, 2015, **5**, 1500963.

10 T. Leijtens, K. Bush, R. Cheacharoen, R. Beal, A. Bowring and M. D. McGehee, Towards enabling stable lead halide perovskite solar cells; interplay between structural, environmental, and thermal stability, *J. Mater. Chem. A*, 2017, **5**, 11483–11500.

11 M. Boskabady, N. Marefati, T. Farkhondeh, F. Shakeri, A. Farshbaf and M. H. Boskabady, The effect of environmental lead exposure on human health and the contribution of inflammatory mechanisms, a review, *Environ. Int.*, 2018, **120**, 404–420.

12 R. A. Michaels, Legacy Contaminants of Emerging Concern: Lead (Pb), Flint (MI), and Human Health, *Environ. Claims J.*, 2020, **32**, 6–45.

13 A. Abate, Stable Tin-Based Perovskite Solar Cells, *ACS Energy Lett.*, 2023, **8**, 1896–1899.

14 F. Igbari, Z. Wang and L. Liao, Progress of Lead–Free Halide Double Perovskites, *Adv. Energy Mater.*, 2019, **9**, 1803150.

15 A. E. Maughan, A. M. Ganose, D. O. Scanlon and J. R. Neilson, Perspectives and Design Principles of Vacancy-Ordered Double Perovskite Halide Semiconductors, *Chem. Mater.*, 2019, **31**, 1184–1195.

16 K. Dave, M. H. Fang, Z. Bao, H. T. Fu and R. S. Liu, Recent Developments in Lead–Free Double Perovskites: Structure, Doping, and Applications, *Chem. – Asian J.*, 2020, **15**, 242–252.

17 Y. Wu, X. Li and H. Zeng, Lead–Free Halide Double Perovskites: Structure, Luminescence, and Applications, *Small Struct.*, 2021, **2**, 2000071.

18 D. E. Lee, S. Y. Kim and H. W. Jang, Lead-free all-inorganic halide perovskite quantum dots: review and outlook, *J. Korean Ceram. Soc.*, 2020, **57**, 455–479.

19 J. Cao and F. Yan, Recent progress in tin-based perovskite solar cells, *Energy Environ. Sci.*, 2021, **14**, 1286–1325.

20 M. M. Byranvand, W. Zuo, R. Imani, M. Pazoki and M. Saliba, Tin-based halide perovskite materials: properties and applications, *Chem. Sci.*, 2022, **13**, 6766–6781.

21 H. Min, J. Chang, Y. Tong, J. Wang, F. Zhang, Z. Feng, X. Bi, N. Chen, Z. Kuang, S. Wang, L. Yuan, H. Shi, N. Zhao, D. Qian, S. Xu, L. Zhu, N. Wang, W. Huang and J. Wang, Additive treatment yields high-performance lead-free perovskite light-emitting diodes, *Nat. Photonics*, 2023, **17**, 755–760.

22 G. Nasti, M. H. Aldamasy, M. A. Flatken, P. Musto, P. Matczak, A. Dallmann, A. Hoell, A. Musiienko, H. Hempel, E. Aktas, D. Di Girolamo, J. Pascual, G. Li, M. Li, L. V. Mercaldo, P. D. Veneri and A. Abate, Pyridine Controlled Tin Perovskite Crystallization, *ACS Energy Lett.*, 2022, **7**, 3197–3203.

23 S. Tian, G. Li, R. C. Turnell-Ritson, Z. Fei, A. Bornet, M. K. Nazeeruddin and P. J. Dyson, Controlling Tin Halide Perovskite Oxidation Dynamics in Solution for Perovskite Optoelectronic Devices, *Angew. Chem., Int. Ed.*, 2024, **63**, e202407193.

24 E. W.-G. Diau, E. Jokar and M. Rameez, Strategies To Improve Performance and Stability for Tin-Based Perovskite Solar Cells, *ACS Energy Lett.*, 2019, **4**, 1930–1937.

25 G. I. Costeanu, Beiträge zum Studium der Alkali– und Erdalkali–hexabromostannate (Rb_2SnBr_6, Cs_2SnBr_6 und $BeSnBr_6$ + $10H_2O$), *Ber. Dtsch. Chem. Ges. A/B*, 1927, **60**, 1312–1315.

26 J. A. A. Ketelaar, A. A. Rietdijk and C. H. Van Staveren, Die Kristallstruktur von Ammonium–, Kalium–, Rubidium– und Cäsiumstannibromid, *Recl. Trav. Chim. Pays-Bas*, 1937, **56**, 907–908.

27 S. L. Suib and P. F. Weller, Gel growth of single crystals of some rubidium and cesium tin halides, *J. Cryst. Growth*, 1980, **48**, 155–160.

28 Md. Abdur Razzaq and T. Islam, Optoelectronic study of double perovskite Rb_2SnBr_6: a first principles calculations, *Global J. Mater. Sci. Eng.*, 2020, 1–5.

29 P. D. Sreedevi and P. Ravindran, Revealing the opto-electronic properties of tin-based vacancy ordered double perovskites: K2SnBr6 and Rb2SnBr6, *AIP Conf. Proc.*, 2021, **2369**, 020149.

30 H. Xia, R. Patterson, G. Conibeer and S. Huang, Ab initio study of M_2SnBr_6 (M = K, Rb, Cs): Electronic and optical properties, *EPL*, 2016, **115**, 57002.

31 L. Krache, M. A. Ghebouli, B. Ghebouli, M. Fatmi, T. Chihi and S. I. Ahmed, Structural, Elastic, Electronic and Optical Properties Study of Hexahalometallate Single Crystals X2SnBr6 (X = Rb, Cs), *Acta Phys. Pol., A*, 2023, **143**, 3–11.

32 M. Faizan, K. C. Bhamu, G. Murtaza, X. He, N. Kulhari, M. M. Al-Anazy and S. H. Khan, Electronic and optical properties of vacancy ordered double perovskites A_2BX_6 (A = Rb, Cs; B = Sn, Pd, Pt; and X = Cl, Br, I): a first principles study, *Sci. Rep.*, 2021, **11**, 6965.

33 R. Ganesan, S. P. Vinodhini, R. Arulmozhi and R. Muralidharan, Influence of halogen substitution in double perovskite $Rb_2Sn(Br_{0.75}I_{0.25})_6$ on the photocatalytic degradation of methylene blue dye under visible light irradiation, *J. Mater. Sci.: Mater. Electron.*, 2023, **34**, 151.

34 B. Glockzin, M. S. Oakley, A. Karmakar, A. Pominov, A. A. Mitchell, X. Ma, M. Klobukowski and V. K. Michaelis, Alkali Tin Halides: Exploring the Local Structure of A_2SnX_6 (A = K, Rb; X = Cl, Br, I) Compounds Using Solid-State NMR and DFT Computations, *J. Phys. Chem. C*, 2023, **127**, 7284–7298.

35 S. M. Jain, T. Edvinsson and J. R. Durrant, Green fabrication of stable lead-free bismuth based perovskite solar cells using a non-toxic solvent, *Commun. Chem.*, 2019, **2**, 91.

36 K. M. Boopathi, P. Karuppuswamy, A. Singh, C. Hanmandlu, L. Lin, S. A. Abbas, C. C. Chang, P. C. Wang, G. Li and C. W. Chu, Solution-processable anti-

mony-based light-absorbing materials beyond lead halide perovskites, *J. Mater. Chem. A*, 2017, **5**, 20843–20850.

37 P. Gong, S. Luo, Y. Yang, F. Liang, S. Zhang, S. Zhao, J. Luo and Z. Lin, Nonlinear Optical Crystal $Rb_4Sn_3Cl_2Br_8$: Synthesis, Structure, and Characterization, *Cryst. Growth Des.*, 2018, **18**, 380–385.

38 B. H. Toby and R. B. Von Dreele, GSAS-II: the genesis of a modern open-source all purpose crystallography software package, *J. Appl. Crystallogr.*, 2013, **46**, 544–549.

39 G. M. Sheldrick, A short history of SHELX, *Acta Crystallogr., Sect. A: Found. Crystallogr.*, 2008, **64**, 112–122.